Model-Predictive Cascade Mitigation in Electric Power Systems With Storage and Renewables—Part II: Case-Study

Mads R. Almassalkhi, *Member, IEEE*, and Ian A. Hiskens, *Fellow, IEEE*

***Abstract*—The novel cascade-mitigation scheme developed in Part I of this paper is implemented within a receding-horizon model predictive control (MPC) scheme with a linear controller model. This present paper illustrates the MPC strategy with a case-study that is based on the IEEE RTS-96 network, though with energy storage and renewable generation added. It is shown that the MPC strategy alleviates temperature overloads on transmission lines by rescheduling generation, energy storage, and other network elements, while taking into account ramp-rate limits and network limitations. Resilient performance is achieved despite the use of a simplified linear controller model. The MPC scheme is compared against a base-case that seeks to emulate human operator behavior.**

***Index Terms*—Cascade mitigation, convex relaxation, energy storage, modeling, model predictive control, power system operation, receding horizon, thermal overloads.**

I. Introduction

THIS paper complements Part I [1], which established a novel model-predictive bilevel control scheme for mitigating the effects of large disturbances and cascading failures in electric power systems. Fig. 1 provides an overview of the bilevel hierarchical operation of the system. This bilevel control scheme is designed to combine both economic and security objectives. Level 1 computes an economically optimal set-point schedule $x^{\mathrm{sp}}, u^{\mathrm{sp}}$, which establishes a reference trajectory for Level 2. Level 2 is implemented using model predictive control (MPC) in a receding-horizon fashion. It achieves security by bringing conductor temperatures below limits, and returns the system to optimal economic performance. In particular, it is proven in [1] that a convex relaxation of line losses is tight exactly when line temperatures exceed their limits. This is a necessary condition for the MPC scheme to alleviate unacceptable temperature overloads on transmission lines. The MPC scheme can be summarized as follows:

1) At time k and for the measured system state x_k^{meas} and updated reference signals from Level 1, x^{sp} and u^{sp}, solve an optimal control problem over fixed interval $[k, k+M]$ taking into account current and future constraints. This yields a sequence of optimal open-loop control actions: $\{u[l|k]\}_{l=0}^{M-1}$.
2) Apply the first instance of the open-loop sequence: $u[0|k]$.
3) Measure the system state reached at time $k+1$, x_{k+1}^{meas}.
4) Set $k = k+1$ and repeat step 1).

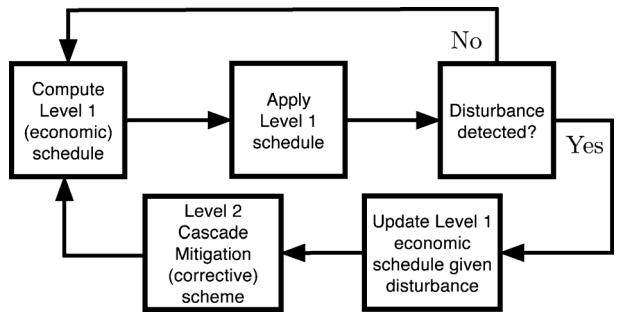

Fig. 1. Overview of the proposed control scheme showing Level 1 (economic) and Level 2 (corrective) interaction.

In order to fully explore the MPC scheme, this paper presents a case-study that is based on the IEEE RTS-96 network [2], with renewables and energy storage (ES) devices added. It highlights practical aspects of the MPC scheme and the role of energy storage in providing improved reliability and economic performance. Specifically, the RTS-96 network is subjected to a large disturbance (i.e., line outage) and the MPC response is analyzed.

The paper is organized as follows. Section II summarizes the MPC model developed in [1]. The representation of the actual power system and the line outage methodology are described in Section III. Section IV formulates a reasonable base-case to emulate the performance of a human operator, explores in detail the case-study and highlights the practicality of the proposed MPC scheme. Concluding remarks are presented in Section V.

II. Controller Model Summary

The controller model is developed in detail in Part I. For the sake of completeness though, a summary is provided here. The Level 2 MPC controller utilizes a sufficient approximation of the non-convex AC power system that is amenable to a quadratic programming (QP) optimization framework. The index l denotes discrete time-steps, and the MPC scheme is employed with prediction and control horizon M. That is, let $l \in \{0, 1, \ldots, M-1\} = \mathcal{M}$.

Manuscript received May 30, 2013; revised October 23, 2013 and February 23, 2014; accepted April 06, 2014. Date of publication June 04, 2014; date of current version December 18, 2014. This work was supported by the U.S. Department of Energy under research grant DE-SC0002283 and by ARPA-E under research grant DE-AR0000232. Paper no. TPWRS-00684-2013.

The authors are with the Department of Electrical Engineering and Computer Science, University of Michigan, Ann Arbor, MI 48109 USA (e-mail: malmassa@umich.edu; hiskens@umich.edu).

Color versions of one or more of the figures in this paper are available online at http://ieeexplore.ieee.org.

Digital Object Identifier 10.1109/TPWRS.2014.2320988

Remark II.1 (Prediction and Control Horizons.): Even though this paper uses identical prediction and control horizons (i.e., $M_p = M = M_c$), it is straightforward to consider the effect of varying either horizon, provided $M_c \leq M_p$.

A power system network can be described in a graph-theoretic sense as consisting of a set of nodes and edges, (i.e., edge $(i,j) \in \mathcal{E}$ for nodes $i,j \in \mathcal{N}$, graph $\mathcal{G} = (\mathcal{E},\mathcal{N})$). Electrical transmission lines have prescribed power flow limits to prevent dangerous sagging and permanent damage (e.g., annealing). These limits are related to the thermal capacity of the conductor and the current flowing through the line. Generally, there is an inverse relationship between the current in a line and the time that may elapse before the line must be taken out of service. In most common overload scenarios, the time-response is on the order of 10–20 min [3].

To ensure secure line flows, it is usual for operators to maintain flows within MVA limits. While it is feasible to take such limits into consideration when determining longer-term energy management schedules (i.e., Level 1), it is unrealistic to expect such constraints to be valid immediately after a significant disturbance (e.g., line outage). This is because flows depend on the physics of the network and (unlike many digital systems) cannot be directly guided, which means that line flows may exceed their limits post-contingency. A more appropriate measure of line overload is the conductor temperature. Therefore, the MPC controller seeks to alleviate temperature overloads.

The states and inputs associated with the proposed formulation of an MPC cascade mitigation scheme for an electric power system are outlined below:

Dynamic States (x): There are three types of dynamic states:
- $\Delta\hat{T}_{ij}$, line (i,j) conductor temperature overload with respect to limit $T_{ij}^{\lim}$;
- E_n, state-of-charge (SOC) for energy storage device n;
- f_{Gn}, power output level for generator n.

Control Inputs (u): The formulation employs six types of control inputs:
- Δf_{Gn}, change to conventional generator n output level;
- f_{GWn}^{spill}, wind spilled from nominal, for wind turbine n;
- f_{Dn}^{red}, demand response (reduced) from nominal, for load n;
- $f_{Qc,n}$, $f_{Qd,n}$, charge (c) and discharge (d) rates for ES n;
- ψ_{ij}, transformer phase shift (rads), for line (i,j).

Uncontrollable Inputs: There are three types of forecast (uncontrollable) inputs (i.e., exogenous disturbances):
- f_{GWn}^{nom}, nominal available power from wind turbine n;
- f_{Dn}^{nom}, nominal demand, for load n;
- d_{ij}, ambient temperature and solar gain, for line (i,j).

Algebraic States (z): Models require nine types of algebraic states:
- f_{ij}, real power flowing through line (i,j);
- f_{ij}^{loss}, real power losses for line (i,j);
- θ_{ij}, phase angle difference between nodes i and j;
- $\theta_{ij}^{+}, \theta_{ij}^{-}$, absolute value approximation of $|\theta_{ij}|$;
- $\{\theta_{ij}^{\text{PW}}(s)\}_{s=1}^{S}$, S-segment PWL approximation of $|\theta_{ij}|^2$;
- f_{GWn}, real power injected by wind turbine n;
- f_{Dn}, real power consumed by load n;
- f_{Qn}, total power injected or consumed by ES n.

Suppose that controls $u(t)$ are step-wise with constant step-width T_s, such that $u(t) := u[k]$ for $t \in [kT_s, (k+1)T_s)$. All discrete dynamics are the result of forward Euler discretization with sample time T_s. For each time k, the dynamic states x_k^{meas} are measured and represent the initial state of the MPC system model. Then, the full MPC formulation is defined as a quadratic programming (QP) problem:

$$\min_{u[l]} \ \left\|x[M] - x_{k+M}^{\text{sp}}\right\|_{S_M} + \sum_{l=0}^{M-1} L(x[l],u[l]) \tag{1a}$$

s.t.

$$\Delta T_{ij}[l+1] = \tau_{ij}\Delta T_{ij}[l] + \rho_{ij}\Delta f_{ij}^{\text{loss}}[l] + \delta_{ij}\Delta d_{ij} \tag{1b}$$

$$E_n[l+1] = E_n[l] + T_s\eta_{c,n}f_{Qc,n}[l] - \frac{T_s}{\eta_{d,n}}f_{Qd,n}[l] \tag{1c}$$

$$f_{Gn}[l+1] = f_{Gn}[l] + \Delta f_{Gn}[l] \tag{1d}$$

$$\Delta\hat{T}_{ij}[l] = \max\{\Delta T_{ij}[l], 0\} \tag{1e}$$

$$0 = f_{Qc,n}[l]f_{Qd,n}[l] \tag{1f}$$

$$0 = a_{ij}x_{ij}^2 f_{ij}^{\text{loss}}[l] - \Delta\theta\sum_{s=1}^{S}(2s-1)\theta_{ij}^{\text{PW}}(s)[l] \tag{1g}$$

$$0 = \theta_{ij}^{+}[l] + \theta_{ij}^{-}[l] - \sum_{s=1}^{S}\theta_{ij}^{\text{PW}}(s)[l] \tag{1h}$$

$$0 = \theta_{ij}^{+}[l] - \theta_{ij}^{-}[l] - (\theta_{ij}[l] - \psi_{ij}[l]) \tag{1i}$$

$$0 = \Gamma_i\left(f_{ij}[l], f_{ij,k}^{\text{loss,est}}, f_{Gn}[l], f_{Dn}[l], f_{Qn}[l], f_{GWn}[l]\right) \tag{1j}$$

$$0 = a_{ij}x_{ij}f_{ij}[l] - (\theta_{ij}[l] - \psi_{ij}[l]) \tag{1k}$$

$$f_{Dn}[l] = f_{Dn}^{\text{nom}}[l] - f_{Dn}^{\text{red}}[l] \tag{1l}$$

$$f_{Qn}[l] = f_{Qc,n}[l] - f_{Qd,n}[l] \tag{1m}$$

$$f_{GWn}[l] = f_{GWn}^{\text{nom}}[l] - f_{GWn}^{\text{spill}}[l] \tag{1n}$$

$$x[l] \in \mathcal{X}, u[l] \in \mathcal{U}, z[l] \in \mathcal{Z} \tag{1o}$$

$$x[M] \in \mathcal{T}_x \tag{1p}$$

$$x[0] = x_k^{\text{meas}} \tag{1q}$$

for all $l \in \mathcal{M}$, where $x[l]$, $u[l]$, and $z[l]$ represent the dynamic state, control input, and algebraic state variables, respectively, at predicted time $k+l$ given initial measured state at time k, x_k^{meas}. This notation has been adopted for clarity of presentation. The more precise forms, $x[l|k]$, $u[l|k]$, and $z[l|k]$, appear in [1]. The terms in the summation of the objective function (1a) are defined by

$$L\left(x[l],u[l]\right) = \left\|x[l] - x_{k+l}^{\text{sp}}\right\|_Q + \left\|u[l] - u_{k+l}^{\text{sp}}\right\|_R \tag{2}$$

where $\|y\|_B \equiv y^\top By$. Also, $S_M \succeq 0, Q \succeq 0$ are non-negative definite weighting matrices, and $R \succ 0$ is a positive definite weighting matrix.

Expressions (1b), (1c), and (1d) represent the linear (discrete-time) dynamics associated with conductor temperature for line (i,j), SOC for energy storage device n, and the power supplied by generator n, respectively. The thermal conductor model is based on the IEEE standard describing the temperature-current relationship in overhead conductors [4]. Temperature dynamics in (1b) are linearized with respect to the conductor temperature ($T_{ij}^{\lim}$ [°C]) obtained for steady-state ampacity ($I_{ij}^{\lim}$ [A]), and conservative ambient parameters. Accordingly, $\Delta T_{ij} = T_{ij} - T_{ij}^{\lim}$ and $\Delta f_{ij}^{\text{loss}} = f_{ij}^{\text{loss}}S_b/(3L_{ij}) - R_{ij}(I_{ij}^{\lim})^2$, where S_b [VA]

and L_{ij} [m] are the three-phase per-unit power base and conductor length, respectively, and R_{ij} [Ω/m] is the resistance per unit length. Appendix A describes the relationship between temperature limit $T^{\lim}$ and ampacity-rated $(I^{\lim})^2R$-losses. Also, $\Delta d_{ij} = d_{ij} - d^*_{ij}$ describes deviations from representative exogenous conditions, ambient temperature T^*_{amb} and solar heat gain rate q^*_s, with q_s a function of conductor diameter and solar conditions. However, it has been assumed for these studies that ambient temperature and solar heat gain rates remain fixed over the period of interest (i.e., $\Delta d_{ij} = 0$).

Constraint (1e) enables the main objective of alleviating temperature overloads while not incentivizing under-loading of lines. That is, MPC should compute control actions that only consider lines with $\Delta T_{ij}[l] > 0$. Keeping in mind the QP formulation, the implementation of this temperature objective can be relaxed to the linear formulation:

$$0 \le \Delta\hat{T}_{ij}[l] \tag{3a}$$
$$\Delta T_{ij}[l] \le \Delta\hat{T}_{ij}[l]. \tag{3b}$$

Because the objective function penalizes $\Delta\hat{T}_{ij}$, this relaxation will always be tight.

The complementarity condition (1f) ensures that energy storage devices cannot simultaneously charge and discharge. As discussed in Part I, exact implementation of complementarity would considerably increase computational complexity. Therefore, the algorithm described in Appendix A of Part I has been adopted for (approximately) enforcing (1f).

A convex piece-wise linear (PWL) approximation of line losses is described by algebraic relations (1g), (1h), and (1i). This PWL relaxation utilizes S segments of width $\Delta\theta = \theta_{\max}/S$ and is modeled using the algebraic states $\theta^+_{ij}, \theta^-_{ij}, \{\theta^{\text{PW}}_{ij}(s)\}^S_{s=1}$. In Part I, it was proven that if a line experiences a temperature overload at predicted time $l+1$, then for all prior time-steps (i.e., $\kappa \le l$) the convex relaxation will be locally tight. When the relaxation is locally tight, the controller has a meaningful and relatively accurate model of line losses, and hence of line temperature. This allows MPC to compute control actions that relieve line overloads.

Equations (1j) and (1k) denote nodal power balance constraints ($\forall i \in \mathcal{N}$) and DC power flows, respectively. Power balance is implied by Kirchhoff's law: power flowing into node i must equal the power flowing out plus/minus that injected/consumed. Note that the term $f^{\text{loss,est}}_{ij,k}$ in (1j) is a constant estimate of line losses at time-step k. It is shown in Part I that by decoupling this loss term from f^{loss}_{ij}, the PWL relaxation inherits crucial tightness properties. The "DC" power flow presented in (1k) reflects application of the "Unified Branch Model" developed in [5]. This unified model provides a consistent formulation for in-phase (IPT, $\psi_{ij} = 0$) and phase-shifting (PST, $a_{ij} = 1$) transformers, and transmission lines ($a_{ij} = 1, \psi_{ij} = 0$).

Algebraic (1l), (1m), and (1n) establish the relationship between control inputs, namely demand response, storage injection/consumption, and wind curtailment, and the power balance of (1j).

The sets defined in (1o) and (1p) are convex polytopes. In particular, $\mathcal{X}$ is closed and $\mathcal{U}$ is compact:

$$\mathcal{X} = \left\{x | E[l] \in [0, \overline{E}]; f_G[l] \in [\underline{f_G}, \overline{f_G}]; \Delta\hat{T}[l] \ge 0\right\} \tag{4}$$
$$\mathcal{Z} = \{z | \theta_{ij}[l] \in [-\theta_{\max}, \theta_{\max}] \subset (-\pi/2, \pi/2)\ ; \ \theta^+_{ij}[l], \theta^-_{ij}[l] \ge 0;\ \theta^{\text{PW}}_{ij}(s)[l] \in [0, \Delta\theta]\} \tag{5}$$
$$\mathcal{U} = \left\{u | f^{\text{red}}_{Dn}[l] \in \left[0, \alpha^{\text{red}}_n\right]\ ; f^{\text{spill}}_{G_W n}[l] \in \left[0, \alpha^{\text{spill}}_n\right]\ ; \ \Delta f_{Gn}[l] \in \left[-T_s R^{\text{down}}_n, T_s R^{\text{up}}_n\right]\ ; \psi_{ij}[l] \in [-\alpha_P, \alpha_P]\ ; \ f_{Qc,n}[l] \in [0, \overline{f}_{Qc,n}]; f_{Qd,n}[l] \in [0, \overline{f}_{Qd,n}]\right\} \tag{6}$$

with bounds defined by appropriate parameters. The sets contain the Level 1 reference trajectories $x^{\text{sp}} \in \mathcal{X}, u^{\text{sp}} \in \mathcal{U}$. Finally, the set $\mathcal{T}_x$ represents the convex polytopic terminal constraint set and is defined by

$$\mathcal{T}_x = \left\{x | \Delta\hat{T}[M] = 0 \wedge x[M] \in \mathcal{X}\right\} \subset \mathcal{X}. \tag{7}$$

Remark II.2 (Terminal Constraint and Feasibility): The addition of the terminal constraint $\mathcal{T}_x$ limits the magnitude of predicted temperature overloads by ensuring that all lines have acceptable temperatures by the end of the horizon. However, terminal constraints may impact the feasibility of the QP problem if the chosen prediction horizon M is too short. In this work, M is appropriately chosen to ameliorate concerns of feasibility.

Given the complete controller model description provided by (1)–(7), the state and input vectors can be defined by

$$x = \text{col}\{\Delta\hat{T}, E, f_G\} \tag{8a}$$
$$u = \text{col}\left\{\Delta f_G, f^{\text{spill}}_{G_W}, f^{\text{red}}_D, f_{Qc}, f_{Qd}, \psi\right\} \tag{8b}$$
$$z = \text{col}\{\theta, \theta^+, \theta^-, \theta^{PW}, f, f^{\text{loss}}, f_D, f_{G_W}, f_Q\}. \tag{8c}$$

Based on the state and input definitions in (8), the weighting matrices in (1a) are given by

$$Q = \text{diag}\left\{p_o I, \frac{p_e}{10M^2} I, \frac{p_g}{10M^2} I\right\} \succ 0 \tag{9a}$$
$$S_M = \text{diag}\{p_o I, p_e I, p_g I\} \succ 0 \tag{9b}$$
$$R = \text{diag}\{p_r I, p_w I, p_s I, p_q I, p_q I, p_p I\} \succ 0 \tag{9c}$$

where I represents identity matrices of appropriate dimensions, $p_\diamond > 0$ are weighting coefficients for states and inputs, and $\text{diag}\{\cdot\}$ denotes a block-diagonal matrix. Note that the terminal cost matrix S_M penalizes deviations from economical references for storage SOC and conventional generation states more severely than does the weighting matrix Q. This is because MPC does not care *how* these reference signals are tracked, only that they are being considered at the end of the horizon.

III. Plant (Actual System) Representation

Over the timescale of interest, the (nonlinear) AC power flow provides an accurate representation of the actual physical power system (i.e., the plant). Therefore, the control actions recommended by MPC, which utilizes the strictly linear model described in Section II, are applied to an accurate AC model of the system at each time-step. In addition, the losses given by the AC power flow are utilized in the nonlinear IEEE standard conductor temperature model to accurately capture the effects of MPC recommendations on the actual system.

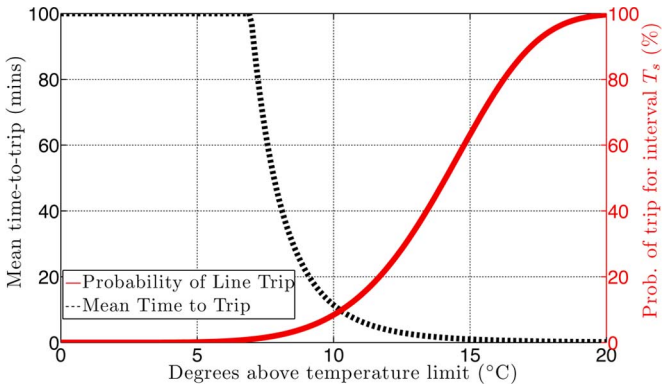

Fig. 2. Probabilistic line outage model. Tripping times above 100 min have been truncated for graphical purposes.

Excessive line temperature (resulting in unacceptable sag) may culminate in line-tripping. The higher the temperature, the more likely line tripping becomes. This inverse relationship between temperature and mean time-to-trip (i.e., mean time-to-failure) is captured in the representation of the actual system by use of the exponential time-to-failure probability density, parameterized by the temperature overload. Thus, given $\Delta T_{ij}[k] > 0$, the probability of line (i,j) tripping during time-step k (over interval T_s) is defined by the resulting cumulative distribution function:

$$P\left(\text{line } (i,j) \text{ trips at } k\right) = 1 - e^{-\lambda(\Delta T_{ij}[k])\, T_s} \qquad (10)$$

where rate parameter $\lambda(\Delta T_{ij}[k]) > 0$ is dependent on the temperature overload. That dependence has been established using the short-term (15-min) emergency (STE) line rating. That is, given an STE rating (e.g., $1.25\times$ nominal rating), the method presented in Appendix A is deployed to compute an associated STE temperature, from which an appropriate $\lambda(\Delta T_{ij}[k])$ is chosen. It has been found experimentally that $\lambda(\Delta T_{ij}[k]) = (\Delta T_{ij}[k]/15)^6$ gives a realistic line-tripping characteristic, as shown in Fig. 2.

Furthermore, considering over-current protection on transmission lines (for large overloads), an additional condition is added to the probabilistic line-tripping model:

$$P\left(\text{line } (i,j) \text{ trips at } k \;\middle|\; \frac{|f_{ij}^{\text{ac}}[k]|}{f_{ij}^{\lim}} \geq \overline{\Omega}\right) = 1 \qquad (11)$$

where f_{ij}^{ac} is the line flow of the actual system (given by the AC power flow), and $\overline{\Omega}$ is an upper bound on the allowable relative instantaneous overload. For example, if $\overline{\Omega} = 3$, then a line flow of 300% of the nominal thermal limit $f_{ij}^{\lim}$ would immediately trip line (i,j).

IV. Case Study: IEEE RTS-96

A. Overview

The hierarchical control scheme developed in Part I [1] and summarized in this paper was applied to an augmented version of the IEEE RTS-96 power system test-case, which is described in full details in [2]. For completeness, a brief overview of this test-case is included here.

TABLE I
Network Model Parameters Used in Case-Study

Model Parameter	Value		Units
Sampling Time, T_s	60		s
3-phase power base, S_b	100		MVA
Energy storage base, E_b	100		MWh
Monetary unit base, M_b	10,000		$
Storage SOC limits, $\overline{E}_i$	2		pu
Storage power limits, $\overline{f}_{Qc}, \overline{f}_{Qd}$	0.25		pu
Nominal wind power, $f_{G_W}^{\text{nom}}$	Fig. 4		pu
Nominal loads, $f_{\text{D}}^{\text{nom}}$	Week 1, day 1 in [2]		pu
Overcurrent protection limit, $\overline{\Omega}$	3		-
Ambient Temperature, T_{amb}	35		°C
Wind speed, angle, $v_w \angle \theta_w$	$0.61, \pi/2$		m/s, rads
Line-to-line base voltage, V_b	138	230	kV
Thermal rating, $f_{ij}^{\lim}$	1.05	3.00	pu
Conductor diameter, D_{ij}	15.5	23.5	mm
Heat capacity, $mC_{p,ij}$	383	916	J/m-°C
Ampacity, $I_{ij}^{\lim}$	439	753	A
Resistance per unit length, R_{ij}	[103,118]	[55,66]	$\mu\Omega$/m
Temperature limit, $T_{ij}^{\lim}$	[62,64]	[67,71]	°C
Temperature coefficient, τ_{ij}	0.796	0.888	-
Loss coefficient, ρ_{ij}	0.157	0.066	°C-m/W
Ambient coefficient, γ_{ij}	0.193	0.104	-
Solar heat gain rate, $q_{s,ij}$	14.4	21.9	W/m

The RTS-96 system consists of 138-kV and 230-kV subsystems. The network is organized into three interconnected physical regions, as illustrated in Fig. 3. It consists of 73 nodes and 120 branches, of which 15 branches are IPTs, one is a PST, and the remainder are overhead transmission lines (138 and 230 kV). Buses are denoted with three digits: the first digit indicates the area while the latter two are intra-area designators. Bus types are indicated by color: generator (blue), load (yellow), and zero-injection (white). Edges represent transmission lines (black) and transformers (aqua/gray). The disturbance is displayed with stars: lines 113–215 and 123–217 were tripped. Note that the three underground cables in the original RTS-96 system have been replaced by equivalent overhead lines to enable application of a single thermodynamic model. Transformer temperature overloading is not considered in this paper, as their thermodynamic models differ from those presented here.

The aim of this case study is to explore the contingency management achievable with the proposed hierarchical control scheme. Unfortunately, the RTS-96 system is designed as a highly reliable system, with unusually high thermal ratings for lines. To bring the system closer to its limits and engender worthwhile scenarios, thermal ratings $f_{ij}^{\lim}$ were reduced by 40%, yielding line temperature limits in the range of 60–70°C. Furthermore, ramp-rates have been reduced by 82.5% to highlight Level 2 performance and enhance the role of storage in congestion management. For the temperature dynamics, the RTS-96 system data only specifies per-unit resistance, reactance and line length, but not the conductor types (i.e., diameter, heat capacity). Therefore, this case-study employed ACSR conductors, 18/1 Waxwing (138 kV) and 26/7 Dove (230 kV), which represent reasonable choices given the reduced line ratings. The parameter values for Dove and Waxwing conductors, along with other system parameters, are provided in Table I. Values in brackets represent ranges.

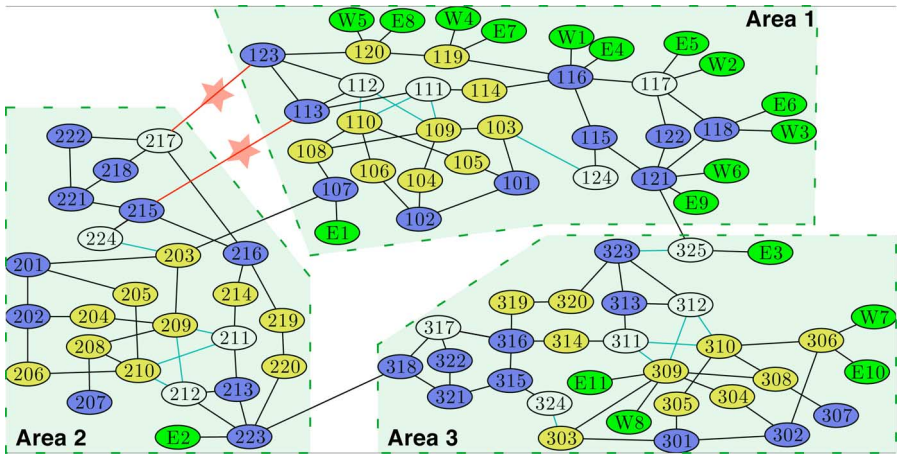

Fig. 3. Modified IEEE RTS-96 network with storage (E) and wind (W) included. Note that storage and wind resources are associated with buses, as indicated in the figure, but the respective edges do not represent transmission lines.

B. Base-Case

To benchmark the performance of the proposed MPC scheme, a base-case controller was developed. This base-case was meant to provide an indication of human operator behavior during a system emergency (disturbance). Clearly, modeling a human operator is non-trivial as standard emergency procedures vary broadly across utilities. Furthermore, the experience of a human operator is not amenable to an implementable (and repeatable) algorithmic framework. However, the formulation presented here captures the underlying goals of the operator:

1) alleviate thermal overloads by rescheduling or curtailing generation, while considering ramp-rate limits and incremental generator cost curves,
2) employ sensitivity-based methods, such as power transmission distribution factors (PTDFs), generation shift factors (GSFs), and transmission loading relief (TLR) procedures to make quick control decisions to relieve thermal overloads [6],
3) shed load as an absolute last resort, and
4) ignore energy storage.

Mapping the above operator response into an MPC-like framework serves as the base-case, and can be implemented as follows:

- Replace $\Delta\hat{T}_{ij}[k]$ with a relative overload metric:

$$\hat{o}_{ij}[k] = 10 \max\left\{0, \left|f_{ij}^{\text{ac}}[k]\right| / f_{ij}^{\text{lim}} - 1\right\}. \qquad (12)$$

  That is, if a line is 25% overloaded, $\hat{o}_{ij} = 2.5$.
- Consider PTDF, GSF, and TLR implicitly as a 1-step MPC process akin to Level 2 (i.e., set $M = 1$) and include overloads $\hat{o}_{ij}[0|k]$, $\hat{o}_{ij}[1|k]$ in the objective and terminal costs.
- Heavily penalize load shedding and adjustment of energy storage levels.
- Remove terminal constraints on overloads, $\mathcal{T}_x$.
- Set weighting matrices $R_{\text{base}} = R, Q_{\text{base}} = S_M$, $S_{M,\text{base}} = S_M$.

C. Optimization Implementation

The objective function weighting factors utilized in MPC Level 2 and the base-case are presented in Table II. Note that for the base-case, the overload coefficient p_o weights the thermal power overload, $\hat{o}_{ij}$, and not temperature. Also, the storage control coefficient for the base-case, $p_q = 1000$, reflects the fact that this resource is not available for decision-making. Generator control actions, Δf_G, are weighted using cost curve parameters,[1] with $p_r = \max\{0.05, a_n/\max_n\{a_n\}\}$ for Level 2, and $p_r = 0.1\max\{0.1, a_n/\max_n\{a_n\}\}$ for the base-case. The cost-curve parameters (a_n, b_n) utilized in this case-study are from [7, Table 1] and are repeated in Table III for completeness. Note that the generator IDs in this table specify their upper output limit, with an ID of Uxx implying $f_{Gn}[k] \le \overline{f_{G_n}} = xx$ MW.

Remark IV.1 [Extension to Unit Commitment (UC)]: Since no minimum generator outputs are specified in [2], lower limits of $\underline{f_{G_n}} = 0$ have been assumed. Consequently, there is no role

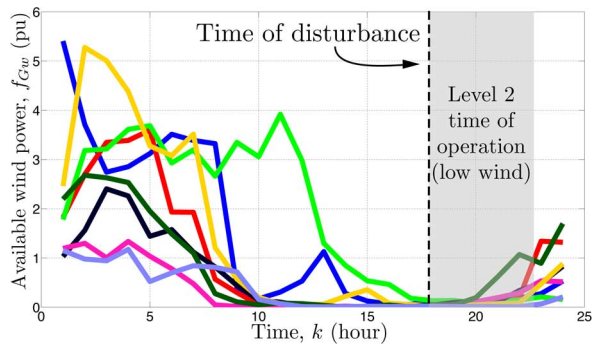

Fig. 4. Hourly wind power profiles for 8 wind turbines in the RTS-96 network over a 24-h horizon.

TABLE II
OBJECTIVE FUNCTION COEFFICIENTS FOR Q, R, S_M MATRICES FOR MPC AND BASE-CASE SYSTEMS

Model	p_o	p_e	p_g	p_r	p_w	p_s	p_q	p_p
Level 2	1	200	200	[0.05,1]	0.15	250	0.2	0.01
Base Case	1	0.01	0.01	[0.01,0.1]	0.5	500	1000	0.1

[1]Recall that the generator cost curves used in Level 1 are of the form: $\text{Cost}(f_{Gn}[k]) = a_n(f_{Gn}[k])^2 + b_n f_{Gn}[k]$.

TABLE III
GENERATOR RAMP-RATE AND COST PARAMETERS

Generator ID	# of units	Ramp rate (pu/hr)	Cost-curve parameters a_n ($/hr-pu^2)	b_n ($/hr-pu)
U12	15	0.105	2.87	1.57
U20	12	0.315	2.1	1.66
U50	18	0.105	0.01	0.11
U76	12	0.210	0.07	0.19
U100	9	0.735	0.22	1.36
U155	12	0.315	0.01	0.182
U197	9	0.315	0.09	1.39
U350	3	0.420	0.01	0.179
U400	6	2.10	0	0.062

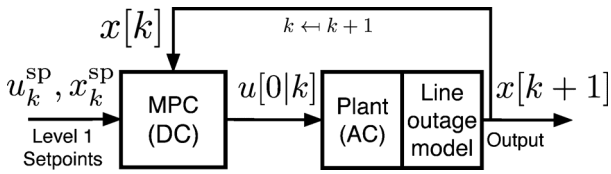

Fig. 5. Interaction of Level 2 MPC with the grid.

for UC in this paper. In a more complete setting, UC could be introduced as a Level 0 process which establishes the set of available generators.

An overview of Level 2 operation is displayed in Fig. 5. Since the early stages of a cascade evolve relatively slowly, significant computation can be performed during that period. Therefore, immediately following a disturbance, Level 1 computes new optimal set-points and passes that updated information to Level 2. This interaction is discussed in detail in Part I.

Note that base-case interactions with the grid have the same form as shown in Fig. 5, except with the Level 2 MPC controller replaced by the MPC-like framework described in Section IV-B.

D. Simulation Results

The case-study was simulated using Matlab to implement Level 1, Level 2, and the base-case. Initially the system was operating economically according to Level 1. However, at hour 18 (low wind, high demand), a double-line outage tripped lines 113–215 and 123–217. Transient (short-term) stability was assumed. Performance and behavior of the Level 2 MPC (with horizon lengths of $M = 5, 10, 20, 30$, and 45) and the base-case are discussed below.

The double-line outage caused the remaining inter-area transmission line 107–203 to become severely overloaded (greater than $1.25 f_{ij}^{\lim}$). The Level 2 MPC scheme alleviated the temperature overloads and brought the system safely to the updated economic set-points provided by Level 1. In contrast, the base-case underwent a cascading failure, with line tripping bringing the system to a voltage collapse after 29 min, as exemplified by non-convergence of the AC power flow. The base-case cascading failure evolved as follows:

- $k = 3$: line 107–203 tripped at $\Delta T_{ij}[3] = 13.5°\mathrm{C}$;
- $k = 16$: line 114–116 tripped at 8.1°C;
- $k = 26$: line 113–123 tripped at 11.4°C;
- $k = 28$: lines 103–109 and 112–123 tripped at 16.8°C and 20.7°C, respectively;

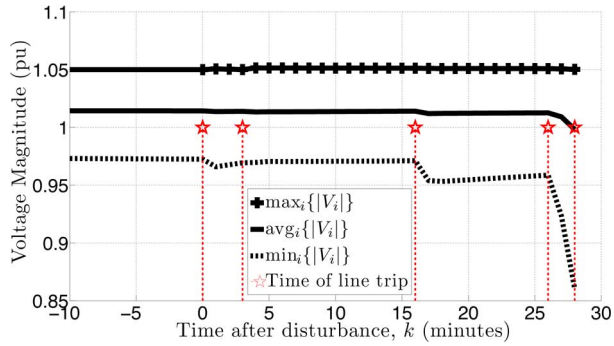

Fig. 6. Base-case operation: voltages undergo cascading failure, resulting in voltage collapse.

- $k = 29$: voltage collapse "Blackout".

This process is illustrated in Fig. 6, where it can be seen that the minimum voltage magnitude fell below 0.87 pu.

The maximum line temperatures for the base-case and MPC are illustrated in Fig. 7(a). Note that MPC is able to avoid excessively high temperatures, and in fact drives all line temperatures below their respective limits by around minute $k \approx 75$. Later, a few lines hover slightly above their temperature limits. However, this is due to model inaccuracy arising from MPC's use of an approximate linear temperature model and the DC power flow. In particular, over that latter phase, the largest temperature deviations above limits are associated with 138-kV lines that exhibit $X/R = 3.83 < 4$. This relatively low X/R ratio engenders errors in the DC approximation of the nonlinear AC network equations. The DC model incorrectly informs the controller that losses are sufficiently low, implying that negligible control action is required for the temperature to drop below its limit in the next time-step. But the actual power system, described by the AC power flow, has higher than predicted losses, and the temperature stays slightly above the limit. The controller repeats these incorrect estimates of losses until control action is required for other reasons, or load patterns autonomously reduce line loadings below limits.

The ability of MPC to eliminate line overloads can be observed in Fig. 7(b), which shows the maximum of the normalized line loadings, $\max_{ij}\{(\text{apparent power})_{ij}/f_{ij}^{\lim}\} \times 100\%$. For $k > 50$, all line loadings are less than 5% above their thermal ratings, which is within expected error levels [8], [9]. These results suggest that despite the presence of approximate models, the MPC scheme is able to reject the disturbance through feedback and return the system to an acceptable state. Further discussion of the impact of model approximations is provided in Section IV-E.

As discussed in Section II, the control actions available to Level 2 MPC for reducing line temperatures include: load reduction, wind curtailment, and energy storage injections. Fig. 7(c) and (d) illustrates the main controls employed to alleviate excessive temperatures for this case-study. Contrasting MPC response with the base-case, it is clear that load and energy storage controls were crucial immediately following the disturbance. By initially reducing the aggregate load by less than 5% [Fig. 7(c)] and curtailing energy storage discharge [Fig. 7(d)], line temperatures were brought to within their limits. For $k \in [75, 240]$,

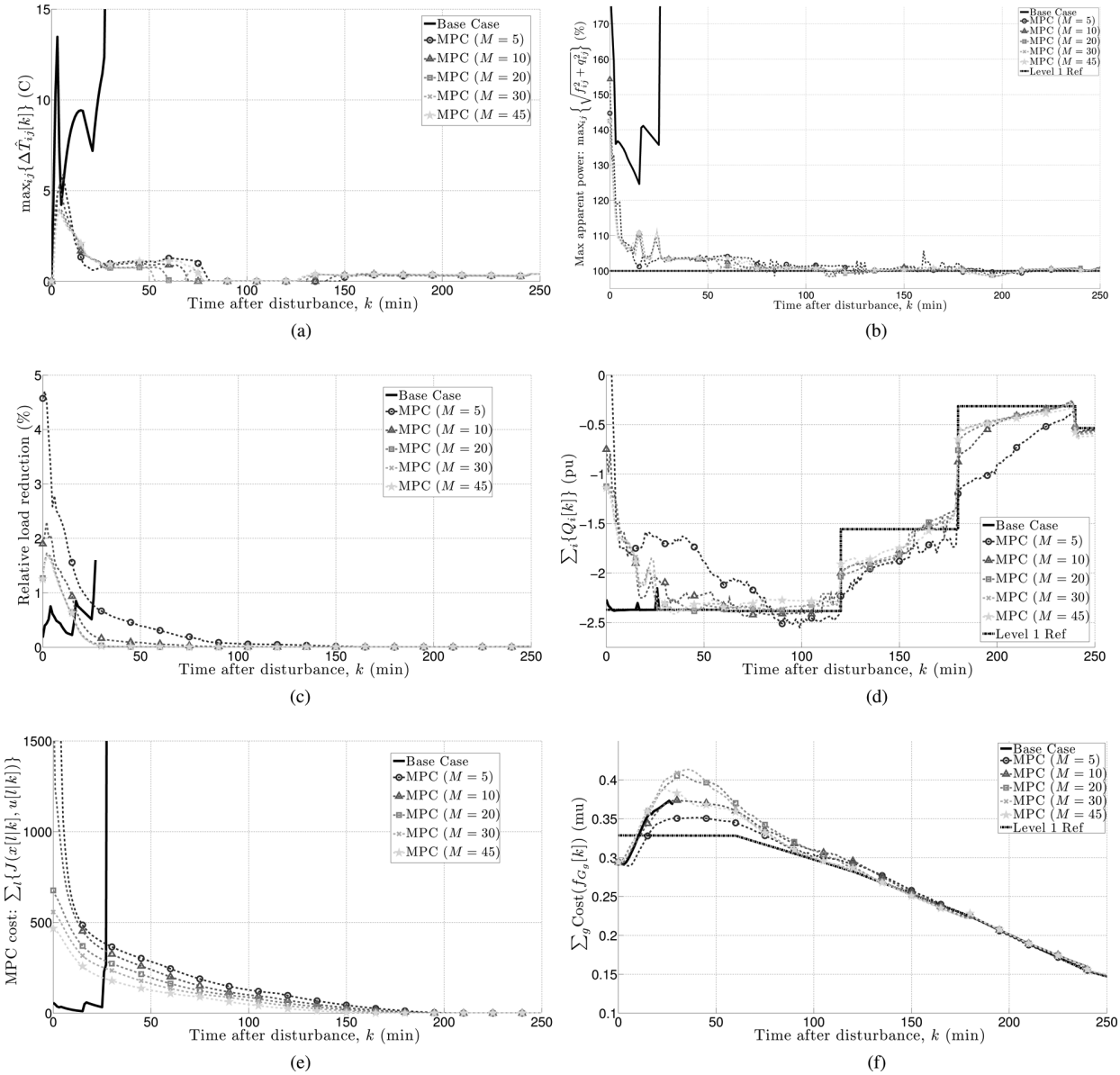

Fig. 7. Case-study simulation results for MPC and the base-case. (a) Maximum line temperature responses. (b) Relative line flow response. "Level 1 Ref" implies line limit. (c) Aggregate load control. (d) Aggregate energy storage charging and discharging. (e) Total MPC objective function value. (f) Total cost of generation with reference to level 1.

TABLE IV
AVERAGE QP SOLUTION TIME PER TIME-STEP k, FOR PREDICTION HORIZON M

QP with horizon M	5	10	20	30	45
Average Time (sec)	0.8	2.1	5.0	9.0	16

storage discharge exceeded reference levels in order to bring SOC back to economical reference levels. Wind curtailment was employed as cheap control over the longer term to bring and keep line temperatures below their limits.

Fig. 7(e) illustrates that the objective function cost (1a), calculated for each MPC run, decreased monotonically over time. This does not prove stability, but highlights the Lyapunov-like properties of the objective function [10] as MPC drives the system back to the Level 1 (economically optimal) equilibrium point.

Level 2 MPC performs a balancing act between ensuring safety criteria and restoring economically optimal set-points. This balance is highlighted in Fig. 7(f), where the cost of conventional generation is shown for both MPC and the base-case. To ensure acceptable line temperatures, MPC initially sacrifices economic optimality by deviating from the Level 1 set-points. For $k > 120$, the system returns to economically optimal levels, with inaccuracy in the MPC model causing some minor discrepancies. Interestingly, over the first 15 min or so, the generation cost achieved by MPC is actually less than the optimal cost given by Level 1. Two factors contribute to this apparent anomaly. Firstly, Fig. 7(f) shows the post-disturbance Level 1 schedule, whereas the generators were initially operating according to less-costly pre-disturbance set-points. Secondly, the updated Level 1 reference schedule enforces hard line-flow constraints, while MPC allows line flows to temporarily exceed limits.

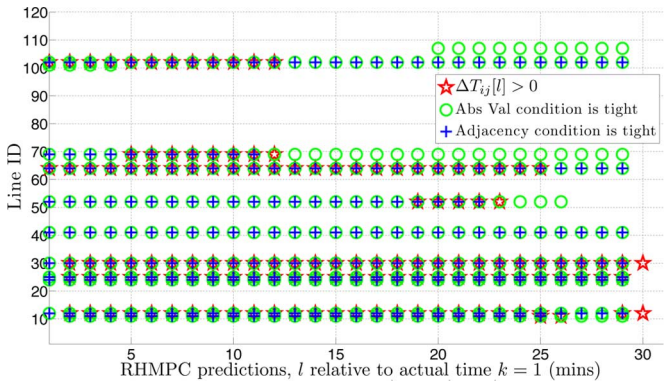

Fig. 8. Illustration that $\Delta T_{ij}[l+1] > 0$ is a sufficient condition for ensuring a locally tight formulation of line losses for all prior time-steps ($\kappa \leq l$).

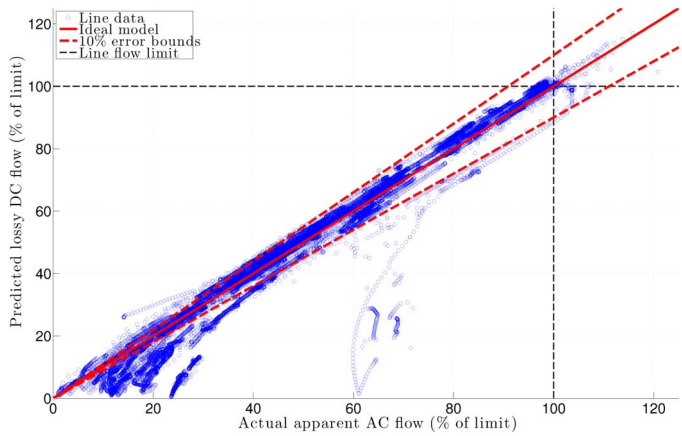

Fig. 9. Accuracy of DC model flows.

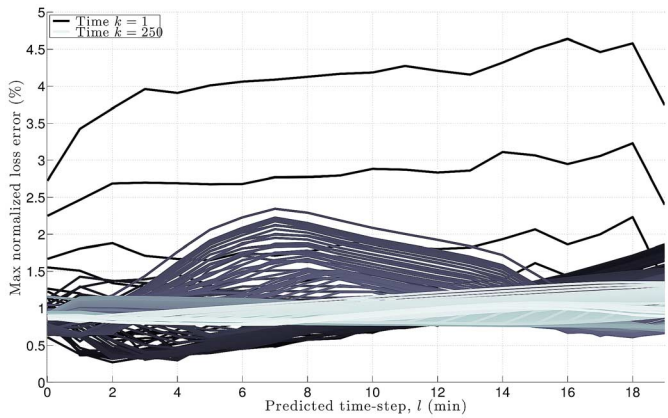

Fig. 10. Maximum loss error: $\max_{ij}\{|f_{ij}^{\text{loss}}[l|k] - f_{ij,k}^{\text{loss,est}}|/f_{ij}^{\text{lim}}\}$.

It is worth pointing out the effect on performance of varying the prediction and control horizon M. Assuming the QP problem remains feasible, employing the terminal constraint $\mathcal{T}_x$ requires that MPC restore line temperatures to within their limits by the end of the horizon. Therefore, as the prediction horizon decreases, the MPC scheme utilizes more aggressive control actions to alleviate overloads. This can be clearly seen in the load-control trajectories of Fig. 7(c).

Furthermore, with a shorter horizon M and the terminal constraint requiring greater use of expensive load and storage control, the MPC enjoys smaller departures in generation from the Level 1 economic reference. Such an outcome is displayed in the generation costs of Fig. 7(f). In addition, it could be argued that for $M > 20$, any performance improvement gained by increasing M is negligible compared with the increased computational cost of solving the open-loop QP problem. Table IV gives average QP solution times for different values of M.

Finally, Fig. 8 illustrates the locally tight nature of the convex relaxation that underpins the controller model's line loss calculation. The figure presents the adjacency, absolute-value and temperature conditions for MPC predictions over the horizon $l \in \mathcal{M}$, with $M = 30$, and with initial conditions corresponding to time-step $k = 1$. Notice how a predicted temperature overload at a time $l + 1$ yields a tight solution for all previous time-steps $\kappa \leq l$. For example, line 52 (207–208) is predicted to have a temperature overload for $l \in [19, 23]$, so adjacency and absolute value relaxations are tight for all $l < 23$. Note that when the temperature deviation of line (i, j) is predicted to remain at or below 0°C for all subsequent time-steps ($l \geq 23$), fictitious losses can occur over those time-steps but have no effect on the objective function. Since fictitious losses are decoupled from the network model, these losses have no effect on network power flows. Thus, fictitious line losses cannot affect control actions when the line temperature is no longer predicted to violate its limit.

E. Model Approximations

Fig. 9 provides insights into the accuracy of the DC power flow model used by MPC. The figure allows a comparison between the line loadings predicted by the lossy DC line model and the apparent-power loadings given by the accurate AC model. The DC flow model is generally within ±10% of the true value, though accuracy is reduced when reactive power makes a relatively significant contribution to the line flow. This situation occurs mainly when active power flows are quite low and lines are well below their ratings. These lines do not, therefore, impact the actions of the DC-based control scheme.

It is also interesting to consider the impact of the constant-loss approximation in (1j). This can be achieved by defining the normalized error

$$\text{Error}_{ij}[l|k] = \frac{\left| f_{ij}^{\text{loss}}[l|k] - f_{ij,k}^{\text{loss,est}} \right|}{f_{ij}^{\text{lim}}}, \quad \forall\, l = 0, 1, \ldots, M-1 \qquad (13)$$

for every line (i, j) and each time-step k. Fig. 10 shows $\max_{ij}\{\text{Error}_{ij}[l|k]\}$ over the prediction horizon $M = 20$, with each curve corresponding to a particular value of time-step k. The shades indicate the progression of time, from black representing $k = 1$ through to white for the final time $k = 250$. It should be mentioned that only one line (107–203) exhibits loss errors greater than 2.5%. This line becomes heavily overloaded immediately upon the initial two-line outage. With this large overload (and correspondingly high losses), MPC actively seeks to reduce the line's losses, which causes $f_{ij,k}^{\text{loss,est}}$ to overestimate losses by less than 5%. However, for

$k \geq 3, \text{Error}_{ij}[l|k] < 2.5\%$ for all lines (i,j), all prediction times $l|k$, and all time-steps k. Furthermore, it was found that average line errors

$$\frac{1}{\text{no. of lines}} \sum_{ij} \text{Error}_{ij}[l|k] < 0.2\% \tag{14}$$

for all $l|k$, and all k. This implies that the error introduced by the constant-loss approximation is negligible for most lines.

V. Conclusions and Future Work

Part I presented a novel model-predictive contingency management scheme that balances economic and security objectives via a bilevel hierarchical control structure. This scheme employs a receding-horizon model predictive control (MPC) strategy that guides the post-disturbance system to a secure, economic state. In determining optimal control decisions, MPC exploits the thermal overload capability of transmission lines. The characteristics of this MPC strategy have been explored in Part II through a case study based on the IEEE RTS-96 test system. This study showed that MPC made very effective use of generation rescheduling, demand response, energy storage adjustment and wind curtailment to eliminate line overloads and restore economic operation. In contrast, a base-case that emulated current operational practices exhibited cascading line outages, and ultimately underwent voltage collapse. The utility of the proposed MPC-based control scheme is illustrated clearly via the case-study. Further work is required, though, to adapt the scheme for larger networks, and to incorporate a more detailed network model [11].

The proposed bilevel control structure separates the economic set-point evaluation of Level 1 from the MPC tracking control of Level 2. Whilst this arrangement is consistent with standard MPC practice [12], the implied time-scale decoupling between levels can limit performance. Economic MPC [13] may offer a framework for systematically evaluating alternative structures. Furthermore, MPC control decisions are quite dependent upon the tuning of the Q, R and S_M weighting matrices. For example, different load-control strategies could be evaluated by adjusting the respective weighting factors. More generally, an automated process for balancing the control objectives is desirable, with [14] offering an appealing approach.

The bilevel control scheme can be used in an offline mode to evaluate economic and resiliency benefits of energy storage and demand response. This approach offers valuable guidance in assessing siting and sizing options for such resources, particularly as uncertainty in renewable generation can be taken into account.

Appendix A
Calculating Current and Temperature Limits

Given the steady-state (continuous) thermal rating of a three-phase transmission line, $f^{\lim}$ [VA], and the base voltage, V_b [V], line ampacity, $I^{\lim}$ [A], is given by

$$I^{\lim} = \frac{f^{\lim}}{\sqrt{3}V_b}. \tag{15}$$

Furthermore, given the per-unit-length series resistance R and other physical conductor parameters, and representative estimates of exogenous parameters (i.e., solar, wind, and air), the per-unit-length heat loss and gain rates at steady-state give the heat balance equation:

$$q_s + R(I^{\lim})^2 = \eta_c(T - T_{\text{amb}}) + \eta_r\left((T+273)^4 - (T_{\text{amb}}+273)^4\right). \tag{16}$$

This provides the temperature limit of the conductor, which is denoted $T^{\lim}$. No closed-form solution exists for (16) as it is quartic with respect to T, so numerical methods must be utilized.

Acknowledgment

The authors would like to thank Prof. D. Kirschen, Dr. H. Pandzic, T. Qiu, Y. Wang, and Dr. M. Xu for many fruitful discussions, and for making available the RTS-96 system data, including wind generation profiles and placement. Furthermore, the authors would like to thank J. Ausmus of WECC for help in selecting suitable conductors.

References

[1] M. Almassalkhi and I. Hiskens, "Model-predictive cascade mitigation in electric power systems with storage and renewables—part I: Theory and implementation scheme," *IEEE Trans. Power Syst.*, vol. 30, no. 1, pp. 67–77, Jan. 2015.

[2] C. Grigg *et al.*, "The IEEE reliability test system," *IEEE Trans. Power Syst.*, vol. 14, no. 3, pp. 1010–1020, Aug. 1999.

[3] P. Kundur, *Power System Stability and Control*, 1st ed. New York, NY, USA: McGraw-Hill Education, 1994.

[4] *IEEE Standard for Calculating the Current-Temperature of Bare Overhead Conductors*, IEEE Std. 738, 2007.

[5] A. Monticelli, *State Estimation in Electric Power Systems: A Generalized Approach*. New York, NY, USA: Springer, 1999.

[6] Manual on Transmission Operations, tech. rep., PJM, Dec. 2012, Operations Support Division.

[7] H. Chavez and R. Baldick, "Inertia and governor ramp rate constrained economic dispatch to assess primary frequency response adequacy," in *Proc. Int. Conf. Renewable Energies and Power Quality*, Mar. 2012.

[8] T. J. Overbye, X. Cheng, and Y. Sun, "A comparison of the AC and DC power flow models for LMP calculations," in *Proc. Hawaii Int. Conf. System Sciences*, Jan. 2004.

[9] B. Stott, J. Jardim, and O. Alsaç, "DC power flow revisited," *IEEE Trans. Power Syst.*, vol. 24, no. 3, pp. 1290–1300, Aug. 2009.

[10] D. Mayne, J. Rawlings, C. V. Rao, and P. O. M. Scokaert, "Constrained model predictive control: Stability and optimality," *Automatica*, vol. 36, no. 6, pp. 789–814, 2000.

[11] C. Coffrin and P. Van Hentenryck, "A linear programming approximation of AC power flows," *INFORMS J. Comput.*, to be published.

[12] E. F. Camacho and C. Bordons, *Model Predictive Control*, 2nd ed. London, U.K.: Springer-Verlag, 2004.

[13] D. Angeli, R. Amrit, and J. Rawlings, "On average performance and stability of economic model predictive control," *IEEE Trans. Autom. Control*, vol. 57, no. 7, pp. 1615–1626, 2012.

[14] V. M. Zavala and A. Flores-Tlacuahuac, "Stability of multiobjective predictive control: A utopia-tracking approach," *Automatica*, vol. 48, pp. 2627–2632, Jul. 2012.

Mads R. Almassalkhi (S'06–M'13) received the B.S. degree in electrical engineering with a dual major in applied mathematics from the University of Cincinnati, Cincinnati, OH, USA, in 2008, and the M.S. degree in Electrical Engineering: Systems from the University of Michigan, Ann Arbor, MI, USA, in 2010, where he received the Ph.D. degree in 2013.

His research interests include controls, optimization, power system analysis, and energy system modeling.

Dr. Almassalkhi is a member of the IEEE Control Systems Society and the IEEE Power & Energy Society.

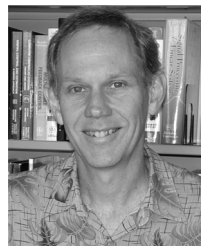

Ian A. Hiskens (F'06) received the B.Eng. degree in electrical engineering and the B.App.Sc. degree in mathematics from the Capricornia Institute of Advanced Education, Rockhampton, Australia, in 1980 and 1983 respectively, and the Ph.D. degree in electrical engineering from the University of Newcastle, Australia, in 1991.

He is the Vennema Professor of Engineering in the Department of Electrical Engineering and Computer Science, University of Michigan, Ann Arbor, MI, USA. He has held prior appointments in the Queensland electricity supply industry, and various universities in Australia and the United States. His research interests lie at the intersection of power system analysis and systems theory. His recent activity has focused largely on integration of renewable generation and controllable loads.

Dr. Hiskens is actively involved in various IEEE societies, and is VP-Finance of the IEEE Systems Council. He is a Fellow of Engineers Australia and a Chartered Professional Engineer in Australia.